# Dalton Transactions

Accepted Manuscript



This is an *Accepted Manuscript*, which has been through the Royal Society of Chemistry peer review process and has been accepted for publication.

Accepted Manuscripts are published online shortly after acceptance, before technical editing, formatting and proof reading. Using this free service, authors can make their results available to the community, in citable form, before we publish the edited article. We will replace this Accepted Manuscript with the edited and formatted Advance Article as soon as it is available.

You can find more information about *Accepted Manuscripts* in the **Information for Authors**.

Please note that technical editing may introduce minor changes to the text and/or graphics, which may alter content. The journal's standard <u>Terms & Conditions</u> and the <u>Ethical guidelines</u> still apply. In no event shall the Royal Society of Chemistry be held responsible for any errors or omissions in this *Accepted Manuscript* or any consequences arising from the use of any information it contains.



**RSCPublishing** 

#### **ARTICLE**

# **Highly Stable and Sensitive LnMOF Ratiometric Thermometers Constructed with Mixed Ligands**

Cite this: DOI: 10.1039/x0xx00000x

Yongqin Wei, Rongjian Sa, Qiaohong Li and Kechen Wu\*

Received ooth January 2012, Accepted ooth January 2012

DOI: 10.1039/x0xx00000x

www.rsc.org/

The mixed-lanthanide metal-organic frameworks (M'LnMOFs) applied for accurate, non-invasive and self-reference temperature measurements have been only recently recognized. It is a great challenge for chemists to fulfil thermostable structure, intense luminescence and high temperature sensitivity on one LnMOF ratiometric thermometer for the thermometric applications. Choosing 2,4-(2,2':6',2''-terpyridin-4'-yl)-benzenedisulfonic acid (H<sub>2</sub>DSTP) as the first ligand and changing ancillary ligand oxalic acid (OA) or 1,4-benzene dicarboxylic acid (BDC), we successfully realized two types of highly stable and sensitive thermometers [Tb<sub>1-x</sub>Eu<sub>x</sub>(OA)<sub>0.5</sub>(DSTP)]•3H<sub>2</sub>O and [Tb<sub>1-x</sub>Eu<sub>x</sub>(BDC)<sub>0.5</sub>(DSTP)]•2H<sub>2</sub>O (x=0.01, 0.02) that in addition exhibit brilliant luminescence over a wide temperature range, providing a new strategy to explore luminescence-based M'LnMOF thermometer.

#### 1. Introduction

The rational design and synthesis of metal-organic frameworks (MOFs) has undergone a tremendous development owing to their fascinating structures and functional applications as electronic, magnetic, optical and catalytic materials. Solid-state luminescence is particularly targeted owing to the advantage of their designability that allows the fine-tuning of luminescent properties. In particular, lanthanide metal-organic frameworks (LnMOFs) offer the advantage of rational choice of light-emissive building blocks for both the lanthanide ions or clusters as nodes and the functional organic ligands as linkers. Moreover, the isostructural LnMOFs make it feasible to maintain the original framework topologies *via* doping approach while produce novel luminescent properties.

The search for new materials with temperature-sensing luminescent properties for their application in thermometry is nowadays a very active field.<sup>4</sup> The thermal dependence of phosphor is a noninvasive and accurate alternative technique that provides fast response and high spatial resolution, and works remotely by way of an optical detection system even in biological fluids, strong electromagnetic fields and fast-moving objects.<sup>5</sup> The study on luminescent thermometers at micro- and nanoscale for the microdevices and potential applications in life sciences is nowadays a very hot research topic.<sup>6</sup> On the other hand, the mixed-lanthanide metal-organic frameworks (M'LnMOFs) for thermometers have been only recently realized.<sup>7</sup> The developed M'LnMOFs methodology for luminescent thermometers is based on a thermally driven energy transfer from Tb<sup>3+</sup> to Eu<sup>3+</sup> within the framework solids

and the corresponding emission intensity ratio can be strongly temperature-dependent. Such ratiometric thermometer does not require any additional calibration of luminescent intensity and thus overcomes the drawbacks of most luminescent thermometers based on the temperature-dependent intensity of one transition whose accuracy can be heavily affected by extrinsic factors like fluctuations in excitation rate, detection efficiency, probe concentration, optical occlusion, or other local inhomogeneities that alter absolute intensities.<sup>8</sup>

In theory, we could develop M'LnMOF ratiometric thermometer with high temperature sensitivity by modulating the excited state energy of organic ligand. 7b,7c But apart from high sensitivity, a thermometer for application should be process of other properties such as high thermal stability and efficient luminescence detectable over a wide temperature range. It is well known that LnMOFs are prone to involve coordinated water or other solvent molecule due to large ion radius and high coordination number of trivalent lanthanide ions. The high-energy vibrations around inner coordination sphere will lead to low luminescent efficiency and even luminescent quench of lanthanide ions. 9 Moreover, the LnMOFs will undergo a subtle structural transformation and even collapse of framework skeleton after the loss of coordinated solvent molecule at high temperature, which further results in the irrecoverable luminescence. Thus, M'LnMOF ratiometric thermometers with thermostable structure, intense luminescence and high sensitivity have not been reported. How to fulfil these terms on one M'LnMOF thermometer is a great challenge for chemists.

We have noticed that introduction of ancillary ligands into LnMOFs often results in the higher luminescent intensity due to the multiple beneficial effects: not only are high-energy vibrations removed from inner coordination sphere, increasing observed lifetime, but a better positioning of the excited state with one of the first ligand increases the efficiency of energy transfer. 10,3b Furthermore, extruding the coordinated solvent molecule with ancillary ligand will probably enhance the thermal stabilities of LnMOFs. Nowadays there has no systemic study of ancillary ligand effect on the temperaturedependent luminescence of M'LnMOF thermometer. Choosing a designed 2,4-(2,2':6',2"-terpyridin-4'-yl)-benzenedisulfonic acid (H<sub>2</sub>DSTP) as the first ligand and changing ancillary ligand, we successfully synthesized two types of LnMOFs,  $[Ln(OA)_{0.5}(DSTP)] \cdot 3H_2O$  (Ln-OA-DSTP) and  $[Ln(BDC)_{0.5} - (Ln-OA-DSTP)] \cdot 3H_2O$ (DSTP)]•2H<sub>2</sub>O (Ln-BDC-DSTP) (Ln = Tb, Eu, OA = oxalic acid, BDC = 1,4-benzene dicarboxylic acid). The ratiometric temperature-sensing properties of the corresponding thermometers Tb<sub>1-x</sub>Eu<sub>x</sub>-OA-DSTP and Tb<sub>1-x</sub>Eu<sub>x</sub>-BDC-DSTP (x = 0.01, 0.02) distinctly change with the added ancillary ligand. Moreover, the removing of coordinated water molecule from the inner coordination sphere by ancillary ligand results in the high luminescent efficiencies of the thermometers and the tightbonding polymeric structure leads to their application in the wide temperature-sensing range. The introduction of ancillary ligands into M'LnMOFs provides a new strategy to explore luminescence-based thermometer.

#### 2. Experiment section

#### Materials and measurements

All commercially available chemicals were of analytical reagent grade and used as received without further purification. Elemental analyses for C, H, N and O were carried out on a Vario MICRO CHNOS Elemental Analyzer. Inductively coupled plasma spectroscopy (ICP) was performed on an Ultima2 Inductively Coupled Plasma OES spectrometer. The Tb/Eu ratios were determined by the ICP analysis and ICP samples were prepared by digesting the dry samples into concentrated HCl (30%). Powder X-ray diffraction (PXRD) patterns were collected in the  $2\theta = 5-50^{\circ}$  range on a D/MAX2500 Powder X-ray diffractometer using  $Cu-K_{\alpha}$ radiation ( $\lambda$ =1.5406Å) at room temperature. Thermogravimetric analyses (TGA) were performed on a NETZSCH STA 449C instrument with a heating rate of 10°C/min in nitrogen atmosphere.

Synthesis 2,4-(2,2':6',2"-terpyridin-4'-yl)benzenedisulfonic acid (H2DSTP). Sodium 4-formylbenzene-1,3-disulfonate (7.8g, 25mmol) and 2-acetylpyridine (5.6mL, 50mmol) were dissolved in 100mL ethanol. To this was added, 30% NH<sub>3</sub> solution (5mL) and NaOH (2g, 50mmol). The solution was stirred vigorously at 0-5°C for 3h, after which an yellow precipitate appeared. The stirring was continued at room temperature for two day and more precipitate was obtained. The precipitate was collected by filtration, washed with methanol. The product was dissolved in 30mL ice water. Hydrochloric

acid was added to the solution and the PH value was adjusted to 5, after which a pale-yellow precipitate appeared. The precipitate was collected by filtration, washed with acetone, and oven-dried at 60°C (4.2g, yield: 32% based on Sodium 4formylbenzene-1,3-disulfonate). Anal. Calcd for H<sub>2</sub>STP•3H<sub>2</sub>O: C 48.18, H 4.04, N 8.03, O 27.50. Found: C 47.93, H 4.12, N 8.24, O 27.15. H NMR (DMSO, Fig. S1, ESI†): 8.71 d 2H, 8.66 d 2H, 8.52 s 2H, 8.29 s 1H, 8.03 t 2H, 7.68 d 2H, 7.49 t 2H, 7.23 d 2H.

Syntheses of MOFs  $[Ln(OA)_{0.5}(DSTP)] \cdot 3H_2O$  (Ln-OA-DSTP). Taking Tb-OA-DSTP as an example, oxalic acid (OA, 0.15mmol), 2,4-(2,2':6',2"-terpyridin- 4'-yl)-benzenedisulfonic acid (H<sub>2</sub>DSTP, 0.3mmol), NaOH (0.9mmol), Tb(NO<sub>3</sub>)<sub>3</sub>•6H<sub>2</sub>O (0.35mmol), and water (25mL) were sealed into a Teflon cup. The solution was heated at 180°C for 3 days and then cooled to room temperature. The yellow crystals were collected by filtration and washed with DMF and water (88.6mg, yield: 41% based on H<sub>2</sub>DSTP). Anal. Calcd for [Tb(OA)<sub>0.5</sub>(DSTP)]•3H<sub>2</sub>O: C 36.48, H 2.64, N 5.80, O 24.29. Found: C 36.52, H 2.83, N 5.75, O 24.35.

Syntheses of MOFs  $[Ln(BDC)_{0.5}(DSTP)] \cdot 2H_2O$  (Ln-BDC-DSTP). The MOFs Ln-BDC-DSTP were synthesized similarly to Ln-OA-DSTP except for the use of 1,4-benzene dicarboxylic acid (BDC) to replace oxalic acid.

Syntheses of  $Tb_{1-x}Eu_x$ -OA-DSTP and  $Tb_{1-x}Eu_x$ -BDC-DSTP. The Tb/Eu mixed MOFs were synthesized similarly to Ln-OA-DSTP and Ln-BDC-DSTP, respectively, except for the use of a mixture of Tb(NO<sub>3</sub>)<sub>3</sub>•6H<sub>2</sub>O and Eu(NO<sub>3</sub>)<sub>3</sub>•6H<sub>2</sub>O.

#### Single-crystal structure determination

Suitable single crystals of Ln-OA-DSTP and Ln-BDC-DSTP (Ln = Eu, Tb) were carefully selected and glued to thin glass fibers with epoxy resin. Intensity data for single crystal were collected on a Rigaku Mercury CCD diffractometer with graphite-monochromatized Mo  $K\alpha$  radiation ( $\lambda = 0.71073$ Å). The empirical absorption corrections were performed using the CrystalClear program. 11 The structures were solved and refined on  $F^2$  by full-matrix leastsquares technique using the SHELX-97 program package. 12 Anisotropic thermal parameters were applied to all non-hydrogen atoms. The hydrogen atoms bonded to the carbon atoms of ligands were generated geometrically and the hydrogen atoms of water molecule were located in a difference Fourier map. In the structures of compounds Ln-OA-DSTP, there were extensive areas of residual electron density that could not sensibly be modeled as water molecules.<sup>13</sup> Therefore, they were removed via application of the SQUEEZE function in *PLATON*. The final formulas of the two compounds were determined by combining with elemental analysis. Crystallographic data for the four compounds are listed in table S1 (ESI†).

#### Photoluminescence (PL) Measurements

Microcrystalline samples in the solid state were used for all photoluminescence measurements. The temperature-dependent emission spectra and the decay curves were recorded on an Edinburgh FLS980 fluorescence spectrometer equipped with a Page 3 of 9 Dalton Transactions

Journal Name ARTICLE

450W ozone-free Xenon Arc lamp as light source, triple-grated monochromators for the excitation and emission pathways, and a R928P photomultiplier tube (PMT) for signal detection in the single-photon counting mode. The temperature measurements (77–400K) were performed on a Linkam THMSE600 controller. The overall quantum yields at room temperature were determined by the absolute method using a  ${\rm BaSO_4}$ -coated integrating sphere as sample chamber on an Edinburgh FLS920 fluorescence spectrometer.

#### Results and discussion

#### Structural characterization

Two types of LnMOFs, Ln-OA-DSTP and Ln-BDC-DSTP (Ln = Tb \ Eu) were synthesized under the hydrothermal reaction of Ln(NO<sub>3</sub>)<sub>3</sub>, H<sub>2</sub>DSTP and corresponding ancillary ligand, All structures were determined by using single crystal X-ray crystallography. In the two types of isostructural LnMOFs, ligand DSTP adopts the same coordination mode and uses three chelating nitrogen atoms of terpyridine, bidentate bridging and monodentate sulfonic groups to link four lanthanide ions, forming a 2D Ln-DSTP structure. Ligand OA using two carboxylate groups to link two metal centers is inserted to the 2D Ln-DSTP, resulting in the final 2D polymeric structure of Ln-OA-DSTP (Fig. 1a). The topology can be viewed as a (4,5)connected net with short Schläfli (point) symbol  $\{3.4^3.5^2\}\{3^2.4^4.5^2.6^2\}$  (Fig. 1b). Ligand BDC using two bidentate bridging carboxylate groups to link four metal centers connects the layered Ln-DSTP, resulting in the final 3D polymeric structure of Ln-BDC-DSTP (Fig. 2a). In the compounds Ln-BDC-DSTP, two metal centers are linked by two bridging carboxylate groups and two bridging sulfonic

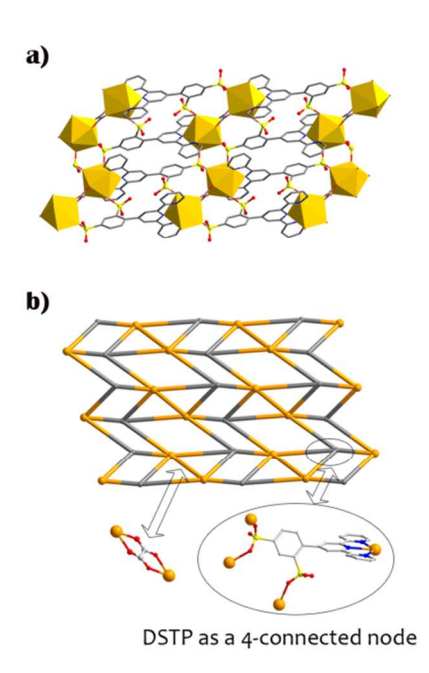


**Fig. 1** The crystal structure of Ln-OA-DSTP: (a) 2D polymeric structure; (b) topological representation.

groups, forming a dimer building block. As shown in Fig. 2b and Fig. 2c, ligand DSTP is simplified as a 3-connected node to link the dimer building blocks and the topology of Ln-BDC-DSTP is a (3,8)-connected net with short Schläfl (point) symbol {4³}2{4<sup>6</sup>.6¹8.8⁴}. The metal centers in Ln-OA-DSTP and Ln-BDC-DSTP adopt a dodecahedron 8-coordinate environment which has no coordinated water and is totally occupied with nitrogen and oxygen atoms of the first ligand DSTP and the ancillary ligand OA or BDC. Such tight-bonding structure is expected to enhance the luminescent efficiency and thermal stability of the corresponding M'LnMOF thermometers.

#### Ratiometric temperature-sensing properties

Because of the tight polymeric structures of as-synthesized materials, they are virtually insoluble in most solvents such as  $H_2O$ ,  $CH_3OH$ ,  $CH_3CN$ , THF, DMF, and DMSO. Microcrystalline samples in the solid state were used for all photoluminescence measurements.

The temperature-dependent emission spectra of Ln-OA-DSTP and Ln-BDC-DSTP (Ln = Tb, Eu) from 77 to 400K are illustrated in Fig. 3. As expected, the emission intensity of  $Tb^{3+}$  in Tb-OA-DSTP and Tb-BDC-DSTP decreases dramatically with increasing temperature. However, the emission intensity of  $Eu^{3+}$  in Eu-OA-DSTP and Eu-BDC-DSTP nearly has no change with increasing temperature. Such significantly different emissions of  $Tb^{3+}$  and  $Eu^{3+}$  will enable us to develop new M'LnMOF thermometers  $Tb_{1-x}Eu_x$ -OA-DSTP and  $Tb_{1-x}Eu_x$ -BDC-DSTP based on the temperature-dependent  $Tb^{3+}/Eu^{3+}$  mission intensity ratio of high sensitivity. Moreover, the successful syntheses of Ln-OA-DSTP and Ln-BDC-DSTP should enable us to investigate the ancillary ligand effect

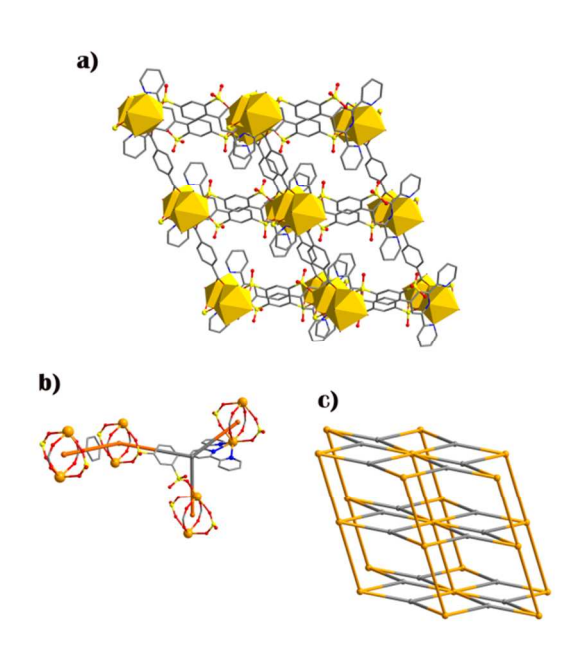


**Fig. 2** The crystal structure of Ln-BDC-DSTP: (a) 3D polymeric structure; (b) linking mode between the dimmer building blocks; (c) topological representation.

the ratiometric temperature-sensing properties. To accomplish the research aims, we synthesized Tb<sub>0.98</sub>Eu<sub>0.02</sub>-OA-DSTP and Tb<sub>0.98</sub>Eu<sub>0.02</sub>-BDC-DSTP with the same molar ratio Tb/Eu, which was confirmed by inductively coupled plasma (ICP) analysis and powder X-ray diffraction (PXRD) measurement (Table S2 and Fig. S2, ESI†). As shown in their temperature-dependent spectra (Fig. 4a and Fig. 5a), the emission intensity of Tb3+ decreases dramatically with increasing temperature, while that of Eu3+ nearly remains unchanged for Tb<sub>0.98</sub>Eu<sub>0.02</sub>-OA-DSTP and even increases gradually for Tb<sub>0.98</sub>Eu<sub>0.02</sub>-BDC-DSTP. The two thermometers exhibit bright photoluminescence to the naked eyes and show different colors (green, yellow, orange, and red) with increasing temperature (Fig. S3, ESI†), allowing us to visualize the temperature change instantly and straightforwardly.

In the temperature-dependent emission spectra of Tb<sub>0.98</sub>Eu<sub>0.02</sub>-OA-DSTP and Tb<sub>0.98</sub>Eu<sub>0.02</sub>-BDC-DSTP,  ${}^5D_0 \rightarrow {}^7F_2$ transitions of Eu<sup>3+</sup> overlap distinctly with <sup>5</sup>D<sub>4</sub>→<sup>7</sup>F<sub>3</sub> transitions of Tb3+ at the cryogenic region (77-225K). Thus, the luminescent intensity of <sup>5</sup>D<sub>0</sub>→ <sup>7</sup>F<sub>2</sub> transition is unfit for being chosen as an experimental parameter to reflect luminescent change of Eu<sup>3+</sup>. It is interesting that the  ${}^5D_0 \rightarrow {}^7F_4$  transitions in the red emissions of Eu-OA-DSTP and Eu-BDC-DSTP have comparable intensity with that of  ${}^5D_0 \rightarrow {}^7F_2$  transitions (Fig. 3). It is well known that in most of Eu(III) compounds, the  $^5D_0 \rightarrow ^7F_2$  transition has by far the largest intensity and the  $^5D_0 \rightarrow ^7F_4$  transition is rather weak. The enhanced intensity of transition  $^{5}D_{0} \rightarrow ^{7}F_{4}$ is also observed  $Na_9[EuW_{10}O_{36}] \cdot 14H_2O^{14}$  and  $[EuCl_3(1,3-Ph(CN)_2]^{15}$ , which was explained as a consequence of the intensity parameters  $\Omega_{\lambda}$ in a highly polarizable environment.<sup>14</sup> In view of no overlap of the  ${}^5D_0 \rightarrow {}^7F_4$  transition with any transition of Tb<sup>3+</sup>, intensity ratio of  ${}^5D_4 \rightarrow {}^7F_5$  transition of Tb<sup>3+</sup> and  ${}^5D_0 \rightarrow {}^7F_4$  transition of Eu<sup>3+</sup> was chosen as the thermometric parameter ( $\Delta = I_{Tb}/I_{Eu}$ ).

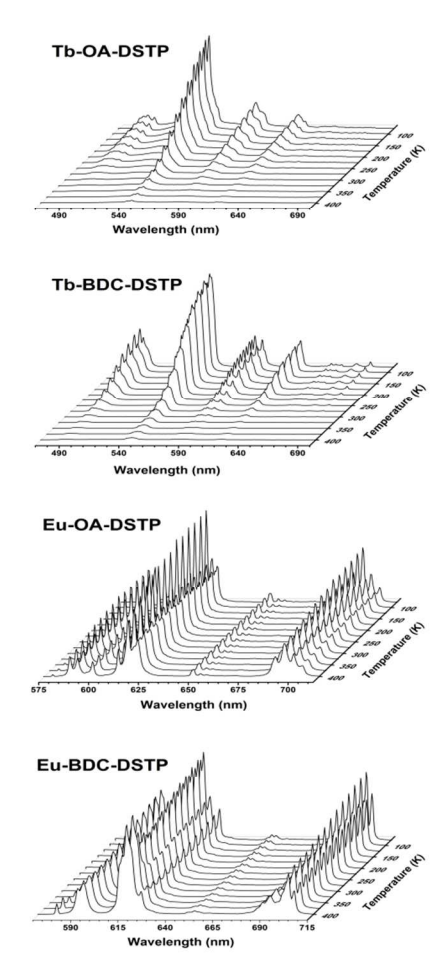
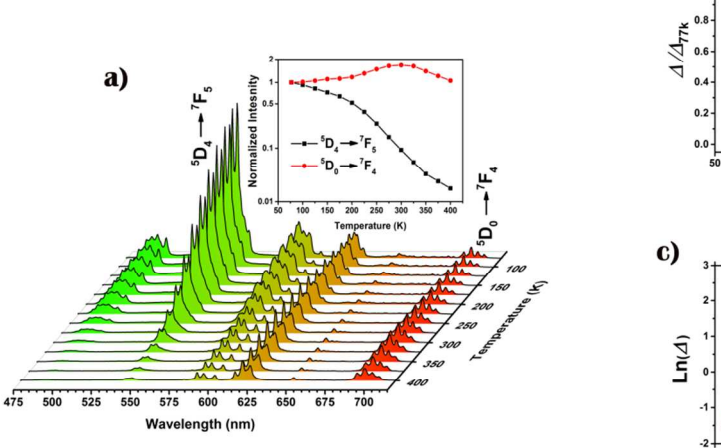
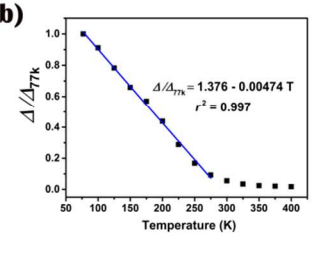


Fig. 3 Emission spectra of Ln-OA-DSTP and Ln-BDC-DSTP (Ln=Tb, Eu) in the solid state recorded between 77 and 400K upon excitation at 360nm.





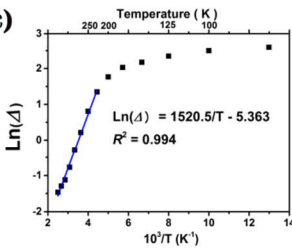
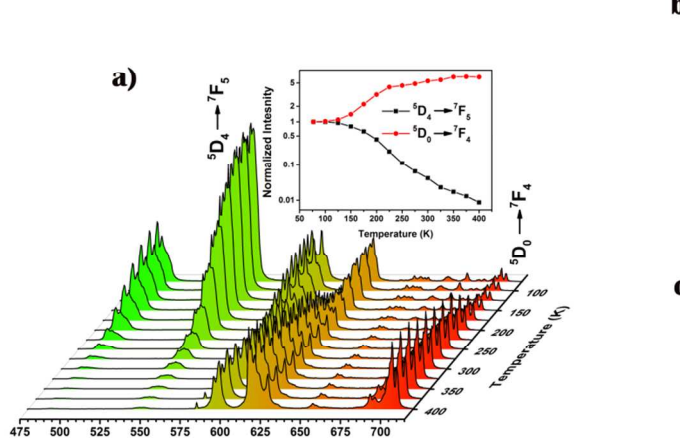
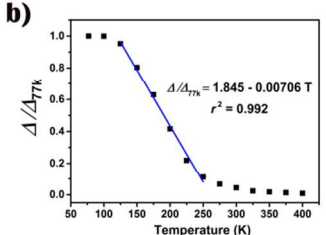


Fig. 4 The ratiometric temperature-sensing properties of Tb<sub>0.98</sub>Eu<sub>0.02</sub>-OA-DSTP: (a) emission spectra for the solid sample recorded between 77 and 400K upon excitation at 360nm, inset: normalized emission intensities of  ${}^5D_4 \rightarrow {}^7F_5$  transition of Tb<sup>3+</sup> (546nm) and  ${}^5D_0 \rightarrow {}^7F_4$  transition of Eu<sup>3+</sup> (696nm); (b) temperature-dependent intensity ratio ( $\Delta/\Delta_{77k}$ ) and linearly fitted curve; (c) the natural logarithm of the thermometric parameter  $\Delta$ changing with the inverse of temperature and the linearly fitted curve.

Page 5 of 9 Dalton Transactions

ARTICLE





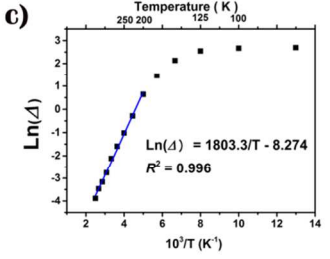


Fig. 5 The ratiometric temperature-sensing properties of  $Tb_{0.98}Eu_{0.02}$ -BDC-DSTP: (a) emission spectra for the solid sample recorded between 77 and 400K upon excitation at 360nm, inset: normalized emission intensities of  ${}^5D_4 \rightarrow {}^7F_5$  transition of  $Tb^{3+}$  (546nm) and  ${}^5D_0 \rightarrow {}^7F_4$  transition of  $Eu^{3+}$  (702nm); (b) temperature-dependent intensity ratio ( $\Delta/\Delta_{77k}$ ) and linearly fitted curve; (c) the natural logarithm of the thermometric parameter  $\Delta$  changing with the inverse of temperature and the linearly fitted curve.

Fig. 4b presents the temperature-dependent intensity ratio of the thermometer  $Tb_{0.98}Eu_{0.02}$ -OA-DSTP. The  $\triangle$  values were normalized to the 77K value (the lowest measured temperature). It is exciting that the temperature measurement can be linearly correlated to experimental parameter in a wide temperature range of 77-275K. Moreover, the sensitivity was calculated based on the equation 1, <sup>16</sup>

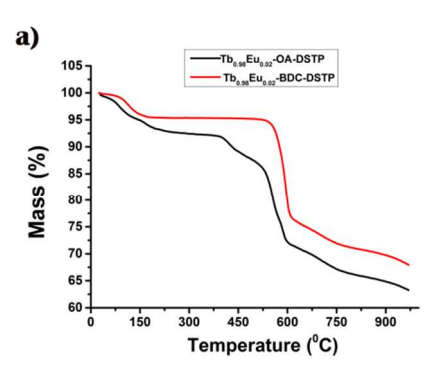
Wavelength (nm)

$$s = \frac{\partial \Delta/\partial T}{\Delta} \tag{1}$$

which showed that the thermometer Tb<sub>0.98</sub>Eu<sub>0.02</sub>-BDC-DSTP has a maximum sensitivity of 2.4% K<sup>-1</sup> at 275K (Fig. S6, ESI†). The first luminescent M'LnMOF thermometer  $[(Tb_{0.9931}Eu_{0.0069})_2 - (DMBDC)_3(H_2O)_4] \cdot DMF \cdot H_2O (DMBDC) =$ 2,5-dimethoxy-1,4-benzenedicarboxylate) reported by Cui et al exhibits a linear correlation between emission intensity ratio and the temperature from 50 to 200K with a maximum sensitivity of 1.3% K-1 at 200K.7a The high sensitivity of thermometer Tb<sub>0.98</sub>Eu<sub>0.02</sub>-OA-DSTP in the wide temperature range is really remarkable, which will allow us to highly sensitize the temperature change. In fact, another thermometer Tb<sub>0.99</sub>Eu<sub>0.01</sub>-OA-DSTP is still process of the excellent linear correlation between the temperature and luminescence intensity ratio from 77 to 225K (Fig. S4b, ESI†), indicating that Tb<sub>1</sub>. <sub>x</sub>Eu<sub>x</sub>-OA-DSTP is a type of very useful luminescent thermometer.

Another notable character of thermometer  ${\rm Tb_{1-x}Eu_x ext{-}OA-DSTP}$  is the higher thermal stability compared with the most of LnMOFs that involve the coordinated water in the inner coordination sphere. As mentioned above, the loss of coordinated water at high temperature will result in irrecoverable luminescence and even collapse of framework skeleton. In result, the most of M'LnMOF thermometers are not fit for being used at the high temperature. In order to confirm the practicability of the two thermometers  ${\rm Tb_{0.98}Eu_{0.02} ext{-}OA-}$ 

DSTP and Tb<sub>0.98</sub>Eu<sub>0.02</sub>-BDC-DSTP at high temperature, we investigate their thermal stabilities. Thermogravimetric analyses (TGA) showed that the two thermometers have decomposition points of 380 and 515°C (Fig. 6a), respectively. The higher stability of Tb<sub>0.98</sub>Eu<sub>0.02</sub>-BDC-DSTP could be attributed to the tight 3D polymeric structure. The first weight



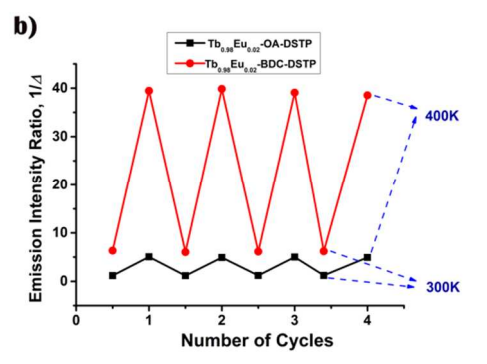


**Fig. 6** The thermal stabilities of the two thermometers of  $Tb_{0.98}Eu_{0.02}$ -OA-DSTP and  $Tb_{0.98}Eu_{0.02}$ -BDC-DSTP: (a) thermogravimetric analyses (TGA); (b) the reversible changes of emission intensity ratio  $1/\Delta$  by the alternative thermo-cycles in the range of 300 and 400 K.

loss of the two thermometers below about 150°C is related to dissociative water molecules in the crystals. But it could not change the framework skeletons. The measured emission intensities and values of the emission intensity ratio remain unchanged, which was verified by the reversible luminescence under thermo-cycles. As shown in Fig. 6b, the reversible changes of the emission intensity ratios of I<sub>Ep</sub>/I<sub>Th</sub> were observed by alternative thermo-cycles in the temperature range of 300 and 400K. It is notable that the verge of temperature-dependent measurement at 400K is far apart from the decomposition points of the two thermometers. But the emission intensity of Tb<sup>3+</sup> decreases dramatically with increasing temperature and the measurement at higher temperature will be unreliable.

The encountered problem is no longer linear correlation of the intensity ratio at elevated temperature because of the low measured value ( $\Delta$ <1). It is necessary to find a new function for the use at high temperature region. We chose the plot of the natural logarithm of the thermometric parameter  $\Delta vs$  the inverse of temperature, which has been adopted by Carlos et al.4e As shown Fig. 4c, for temperatures above 225K the temperature dependence of  $ln(\Delta)$  of thermometer  $Tb_{0.98}Eu_{0.02}$ -OA-DSTP follows the equation:  $ln(\Delta)=1520.5/T-5.363$  $(R^2=0.994)$ . The slope value of 1520.5 is larger than the reported value by a factor of ca. 10. Thus, we successfully developed a new type of thermostable thermometer Tb<sub>1-x</sub>Eu<sub>x</sub>-OA-DSTP being process of not only the high sensitivity but also the wide temperature-sensing range.

As shown in Fig. 5 and Fig. S5 (ESI†), the ratiometric temperature-sensing properties distinctly change with the added ancillary ligand. Tb<sub>1-x</sub>Eu<sub>x</sub>-BDC-DSTP (x=0.01, 0.02) exhibit the remarkably higher maximum sensitivities (2.8% K<sup>-1</sup> at 225K for Tb<sub>0.98</sub>Eu<sub>0.02</sub>-BDC-DSTP and 3.9% K<sup>-1</sup> at 200K for Tb<sub>0.99</sub>Eu<sub>0.01</sub>-BDC-DSTP, larger than that of the corresponding Tb<sub>1-x</sub>Eu<sub>x</sub>-OA-DSTP at the same temperature), Although the thermometric parameters of Tb<sub>1-x</sub>Eu<sub>x</sub>-BDC-DSTP are linearly related in a narrower temperature range, the natural logarithm of the thermometric parameters  $\Delta$  are linearly related to the inverse of temperature in a wide temperature range of 200-400K. The slope values of 1803.3 and 1655.1 are larger than that of the corresponding thermometers  $Tb_{1-x}Eu_x$ -OA-DSTP.

#### Energy transfer mechanism

The measurement for lifetimes of Tb3+ and Eu3+ in the pure MOFs and the Tb/Eu-codoping MOFs (Fig. S7, ESI†) showed that the lifetime of Tb<sup>3+</sup> in the Tb/Eu-codoping MOF becomes shorter compared with that in the pure MOF, whereas the lifetime of Eu<sup>3+</sup> increases. This information indicates the Tb<sup>3+</sup>to-Eu3+ energy transfer, which is verified by the emission spectra of Tb<sub>0.98</sub>Eu<sub>0.02</sub>-OA-DSTP and Tb<sub>0.98</sub>Eu<sub>0.02</sub>-BDC-DSTP upon excitation of 488nm (Fig. S8, ESI † ). The higher sensitivities of Tb<sub>1-x</sub>Eu<sub>x</sub>-BDC-DSTP compared with Tb<sub>1-x</sub>Eu<sub>x</sub>-OA-DSTP (x=0.01, 0.02) are related to the efficient energy transfer from Tb3+ to Eu3+, which is estimated using the equation 2,17

$$\eta_{Tb-Eu} = 1 - \frac{\tau_{obs}}{\tau_{Tb}} \tag{2}$$

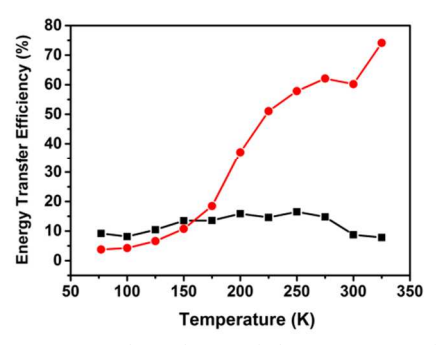
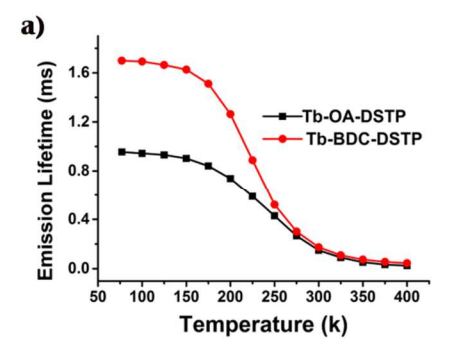


Fig. 7 Temperature-dependence of the energy transfer efficiency  $\eta_{\text{Tb-Eu}}$  of Tb<sub>0.98</sub>Eu<sub>0.02</sub>-OA-DSTP (black, square) and Tb<sub>0.98</sub>Eu<sub>0.02</sub>-BDC-DSTP (red, circle).



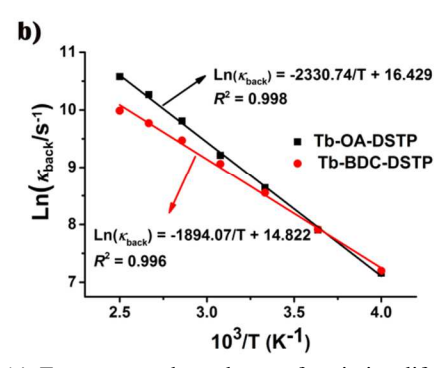


Fig. 8 (a) Temperature-dependence of emission lifetimes and (b) Arrehenius plots for back energy transfer rate constants of Tb-OA-DSTP and Tb-BDC-DSTP.

where  $\tau_{Tb}$  and  $\tau_{obs}$  are the emission lifetimes monitoring  $^5D_4$ emission of Tb<sup>3+</sup> at 546nm of the pure Tb(III) compound and the corresponding Tb/Eu-codoping compound, respectively. As shown in Fig. 7, the energy transfer efficiency of Tb<sub>0.98</sub>Eu<sub>0.02</sub>-OA-DSTP is relatively lower in all temperature range, while  $Tb_{0.98}Eu_{0.02}$ -BDC-DSTP shows different temperaturedependence of the energy transfer efficiency, which enhances quickly with increasing temperature, thus resulting in the quicker enhancement of the emission intensity of Eu3+ and the higher temperature sensitivity.

The difference of temperature sensitivity is essentially related to the triplet-state energy location of ligands. In order to investigate energy transfer between ligands and lanthanide ions,

**ARTICLE** 

Page 7 of 9 Dalton Transactions

the emission spectrum of Gd-OA-DSTP was measured at 77K (Fig. S9, ESI†), which showed that the first triplet-state energy of DSTP (19050cm<sup>-1</sup>, estimated from the phosphorescence peak at about 525nm) is slightly higher than  $^5D_0$  of the Eu<sup>3+</sup>(17200cm<sup>-1</sup>) and lower than  $^5D_4$  of the Tb<sup>3+</sup> (20400cm<sup>-1</sup>). We could deduce that energy transfer to appropriate level of Tb<sup>3+</sup> probably came from the first triplet-state of ancillary ligands OA or BDC. The lower triplet-state energy of BDC compared with that of OA will result in the more efficient energy back transfer and further makes energy transfer from Tb<sup>3+</sup> to Eu<sup>3+</sup> easier. We estimated the energy back-transfer rate ( $\kappa_{\text{back}}$ ) of Tb-OA-DSTP and Tb-BDC-DSTP using kinetic analysis.  $\kappa_{\text{back}}$  is assumed to obey the following Arrhenius-type equation 3, <sup>18</sup>

$$\ln k_{back} = \ln \left( \frac{1}{\tau_{abs}} - \frac{1}{\tau_{77K}} \right) = \ln A - \frac{E_a}{k_B T}$$
 (3)

where  $\tau_{\rm obs}$  is the emission lifetime,  $\tau_{77\rm K}$  is the emission lifetime at 77k,  $E_{\rm a}$  is the activation energy,  $\kappa_{\rm B}$  is the Boltzmann constant and T is the absolute temperature. The activation energies obtained for Tb-OA-DSTP and Tb-BDC-DSTP (Fig. 8) are  $1620\pm26{\rm cm}^{-1}$  and  $1316\pm36{\rm cm}^{-1}$ , respectively, in agreement with the above suggestion that the energy back transfer of Tb<sup>3+</sup> involves the excited state of ancillary ligand.

#### 4. Conclusion

**Journal Name** 

In summary, we successfully target two types of M'LnMOF ratiometric thermometers Tb<sub>1-x</sub>Eu<sub>x</sub>-OA-DSTP and Tb<sub>1-x</sub>Eu<sub>x</sub>-BDC-DSTP (x = 0.01, 0.02) for application by introducing ancillary ligands into the framework solids. The thermometers exhibit brilliant luminescence in the all temperature range of 77-400k. The absolute luminescence quantum yields of Tb<sub>0.98</sub>Eu<sub>0.02</sub>-OA-DSTP and Tb<sub>0.98</sub>Eu<sub>0.02</sub>-BDC-DSTP measured at room temperature are 16.2% and 24.5% respectively. Notably, the overall emission of Tb<sub>1-x</sub>Eu<sub>x</sub>-BDC-DSTP is even more intense at the elevated temperature. The intense luminescence of the thermometers can be explained as a consequence of excellent light-harvesting linker DSTP with large  $\pi$ -conjugated system, efficient energy transfer from Tb<sup>3+</sup> to Eu<sup>3+</sup> and high-energy vibrations removed from the inner coordination sphere by the ancillary ligand OA or BDC. Furthermore, the tight-bonding structure as a result of the introduction of the ancillary ligands enhances the thermal stabilities of the thermometers and leads to their application in the wide temperature-sensing range, which has been seldom reported for M'LnMOF thermometers.7d It is notable that the ratiometric temperature-sensing properties distinctly change with the added ancillary ligand. Although the introduction of ancillary ligands brings difficulty for study on energy transfer mechanism of M'LnMOF thermometers, improving their temperature-sensing properties with ancillary ligands provides a new strategy to explore luminescence-based M'LnMOF thermometers.

#### Acknowledgements

We gratefully acknowledge the financial support of Natural Science Foundation of China (no. 21171165, 21201165 and 91122015).

#### Notes and references

State Key Laboratory of Structural Chemistry, Fujian Institute of Research on the Structure of Matter, Chinese Academy of Sciences, Fujian 350002, People's Republic of China. Email: wkc@fjirsm.ac.cn; Fax: +86-591-83792932

- † Electronic supplementary information (ESI) available: Information of supplementary data and figures. CCDC reference numbers 1016955-1016958.
- (a) S. L. James, *Chem. Soc. Rev.*, 2003, 32, 276-288; (b) A. Bétard and R. A. Fischer, *Chem. Rev.*, 2012, 112, 1055-1083.
- 2 (a) M.D. Allendorf, C. A. Bauer, R. K. Bhakta and R. J. T. Houk, Chem. Soc. Rev., 2009, 38, 1330-1352; (b) Y. Cui, Y. Yue, G. Qian and B. Chen, Chem. Rev., 2012, 112, 1126-1162.
- 3 (a) P. Falcaro and S. Furukawa, Angew. Chem. Int. Ed., 2012, 51, 8431-8433; (b) Y, Wei, Q. Li, R. Sa and K. Wu, Chem. Commun., 2014, 50, 1820-1823.
- 4 (a) X.-D. Wang, O. S. Wolfbeis and R. J. Meier, *Chem. Soc. Rev.*, 2013, 42, 7834-7869; (b) H. S. Peng, M. I. J. Stich, J. B. Yu, L. N. Sun, L. H. Fischer and O. S. Wolfbeis, *Adv. Mater.*, 2010, 22, 716-719; (c) C. D. S. Brites, P. P. Lima, N. J. O. Silva, A. Millan, V. S. Amaral, F. Palacio and L. D. Carlos, *New J. Chem.*, 2011, 35, 1177-1183; (d) X. Yin, F. Meng and L. Wang, *J. Mater. Chem. C.*, 2013, 1, 6767-6773; (e) C. D. S. Brites, P. P. Lima, N. J. O. Silva, A. Millá, V. S. Amaral, F. Palacio and L. D. Carlos, *Nanoscale*, 2013, 5, 7572-7580; (f) D. Jaque and F. Vetrone, *Nanoscale*, 2012, 4, 4301-4326.
- 5 (a) S. W. Allison and G. T. Gillies, *Rev. Sci. Instrum.*, 1997, **68**, 2615-2650; (b) P. Löw, B. Kim, N. Takama and C. Bergaud, *Small*, 2008, **4**, 908-914; (c) A. E. Albers, E. M. Chan, P. M. McBride, C. M. Ajo-Franklin, B. E. Cohen and B. A. Helms, *J. Am. Chem. Soc.*, 2012, **134**, 9565-9568.
- 6 (a) G. Kucsko, P. C. Maurer, N. Y. Yao, M. Kubo, H. J. Noh, P. K. Lo, H. Park and M. D. Lukin, *Nature*, 2013, 500, 54-59; (b) C. Gota, K. Okabe, T. Funatsu, Y. Harada and S, Uchiyama, *J. Am. Chem. Soc.*, 2009, 131, 2766-2767; (c) G. Ke, C. Wang, Y. Ge, N. Zheng, Z. Zhu and C. J. Yang, *J. Am. Chem. Soc.*, 2012, 134, 18908-18911; (d) A. Riedinger, P. Guardia, A. Curcio, M. A. Garcia, R. Cingolani, L. Manna and T. Pellegrino, *Nano Lett.*, 2013, 13, 2399–2406; (e) J.-M. Yang, H. Yang and L. Lin, *ACS Nano*, 2011, 5, 5067-5071; (f) Y. Takei, S. Arai, A. Murate, M. Takabayashi, K. Oyama, S. Ishiwata, S. Takeoka and M. Suzuki, *ACS Nano*, 2014, 8, 198-206.
- 7 (a) Y. Cui, H. Xu, Y. Yue, Z. Guo, J. Yu, Z. Chen, J. Gao, Y. Yang, G. Qian and B. Chen, J. Am. Chem. Soc., 2012, 134, 3979-3982; (b) X. Rao, T. Song, J. Gao, Y. Cui, Y. Yang, C. Wu, B. Chen and G. Qian, J. Am. Chem. Soc., 2013, 135, 15559-15564; (c) Y. Cui, W. Zou, R. Song, J. Yu, W. Zhang, Y. Yang and G. Qian, Chem. Commun., 2014, 50, 719-721; (d) K. Miyata, Y. Konno, T. Nakanishi, A. Kobayashi, M. Kato, K. Fushimi and Y. Hasegawa, Angew. Chem. Int. Ed., 2013, 52, 6413-6416.
- 8 (a) E. J. McLaurin, L. R. Bradshaw and D. R. Gamelin, *Chem. Mater.*, 2013, **25**, 1283-1292; (b) S. Zheng, W. Chen, D. Tan, J. Zhou, Q.

ARTICLE Journal Name

- Guo, W. Jiang, C. Xu, X. Liu and J. Qiu, *Nanoscale*, 2014, **6**, 5675-5679.
- J. L. Krop and M. W. Windsor, *J. Chem. Phys.*, 1965, 42, 1599-1608.
   (a) S. V. Eliseeva, D. N. Pleshkov, K. A. Lyssenko, L. S. Lepnev, J.-C. G. Bünzli and N. P. Kuzmina, *Inorg. Chem.*, 2010, 49, 9300-9311;
   (b) A. Fratini, G. Richards, E. Larder and S. Swavey, *Inorg. Chem.*, 2008, 47, 1030-1036.
- 11 Molecular Structure Corporation and Rigaku, 2000. *CrystalClear*. **Version 1.36**. MSC, 9009 New Trails Drive, The Woodlands, TX 77381-5209, USA, and Rigaku Corporation, 3-9-12 Akishima, Tokyo, Japan.
- 12 (a) G. M. Sheldrick, SHELXS-97, Program for Crystal Structure Solution, University of Göttingen: Göttingen, Germany, 1997; (b) G. M. Sheldrick, SHELXL-97, Program for Crystal Structure Refinement, University of Göttingen: Göttingen, Germany, 1997.
- 13 (a) M. Tominaga, K. Suzuki, M. Kawano, T. Kusukawa, T. Ozeki, S. Sakamoto, K. Yamaguchi and M. Fujita, *Angew. Chem., Int. Ed.*, 2004, 43, 5621-5625; (b) J.-R. Li, A. A. Yakovenko, W.-G. Lu, D. J. Timmons, W.-J. Zhuang, D.-Q. Yuan and H.-C. Zhou, *J. Am. Chem. Soc.*, 2010, 132, 17599-17610.
- 14 R. A. S. Ferreira, S. S. Nobre, C. M. Granadeiro, H. I. S. Nogueira, L. D. Carlos and O. L. Malta, *J. Lumin.*, 2006, **121**, 561-567.
- 15 C. J. Höller, P. R. Matthes, M. Adlung, C. Wickleder and K. Müller-Buschbaum, *Eur. J. Inorg. Chem.*, 2012, 5479-5484.
- 16 A. Cadiau, C. D. S. Brites, P. M. F. J. Costa, R. A. S. Ferreira, J. Rocha and L. D. Carlos, ACS Nano, 2013, 7, 7213-7218.
- 17 (a) C. Piguet, J.-C. G. Bünzli, G. Bernardinelli, G. Hopfgartner and A. F. Williams, *J. Am. Chem. Soc.*, 1993, 115, 8197-8206; (b) M. Xiao and P. R. Selvin, *J. Am. Chem. Soc.*, 2001, 123, 7067-7073.
- 18 G. Blasse and B. C. Grabmaier, *Luminescent materials*, Springer, New York, 1994, 92

## Highly Stable and Sensitive LnMOF Ratiometric Thermometers Constructed with Mixed Ligands

Yongqin Wei, Rongjian Sa, Qiaohong Li and Kechen Wu\*

By introducing ancillary ligands into M'LnMOFs and removing coordinated water molecule from the inner coordination sphere, we successfully realized two types of highly stable and sensitive thermometers that in addition exhibit brilliant luminescence over a wide temperature range, providing a new strategy to explore luminescence-based M'LnMOF thermometer.

